



420 ve 304L Farklı Paslanmaz Çeliklerin TIG Kaynağı Sonrası Radyografik Muayenesi

Radiographic Testing of 420 and 304L Dissimilar Stainless Steels after TIG Welding

Mustafa Gökhan Murat¹ , Aziz Barış Başyigit^{2*} 

¹, Naval Training and Education Command, Turkish Naval Forces, 34676 İstanbul, TURKEY

^{2*}Kırıkkale University, Faculty of Engineering, Department of Metallurgical and Material Engineering, 71450 Kırıkkale, TURKEY

Başvuru/Received: 07/12/2020

Kabul / Accepted: 24/12/2020

Çevrimiçi Basım / Published Online: 18/01/2021

Son Versiyon/Final Version: 18/01/2021

Öz

SAE/AISI 304L östenitik paslanmaz çelikler oksitleyici ortamlardaki korozyon dayanımları için tercih edilirken, SAE/AISI 420 martenzitik paslanmaz çelikler genel olarak atmosferik korozyona karşı dayanım amaçlı kullanılmaktadırlar. Martenzitik paslanmaz çelikler birçok alaşımlı çeliklere yakın değerlerde yüksek mekanik dayanım değerleri sergilerken bunun yanında östenitik paslanmaz çelikler yüksek ve düşük sıcaklıklarda yüksek tokluk değeri ortaya koyarlar. Bu iki farklı alaşım grubu ekonomik koşullar ve mekanik özellik yaklaşımlarından dolayı bir yapıda bir arada kullanılabilirler. Kaynaklı bağlantıların kaynak metalleri ve ısının tesiri altındaki bölgeleri, güvenilir bir kaynaklı bağlantı elde etmek için; penetrant, ultrasonik ve radyografik muayene yöntemleri gibi tekniklerle detaylıca incelenmelidir. Bu çalışmada; 3 mm kalınlıktaki SAE/AISI 304L östenitik paslanmaz çelik levha ile 3mm kalınlıkta SAE/AISI 420 martenzitik paslanmaz çelik levha TIG (Tungsten Asal Gaz) kaynak yöntemiyle saf argon koruyucu gazı altında ER312, ER316L, ER2209 olmak üzere 3 farklı ilave tel kullanılarak birleştirilmiştir. TIG kaynak teli bileşiminin kaynak metalinde oluşabilecek kusurlara etkileri incelenmiştir. Bu amaçla, numunelerin kaynak metallerinin tamamı x- ışınları radyografik muayenesi ile test edilmiştir. ER312 ve ER2209 TIG teli ile birleştirilen numunelere kıyasla, ER 316L TIG teli ile birleştirilmiş olan numunelerin kaynak metalinde, dolgu telinin en düşük krom ve en yüksek nikel içeriğine sahip oluşu neticesinde en düşük miktarda olduğu düşünülen gevrek karbürler bağli olarak en düşük oranda süreksizlik tespit edilmiştir.

Anahtar Kelimeler

“Radyografik muayene, 420 ve 304L paslanmaz çelikler, kaynak metalindeki süreksizlikler”

Abstract

SAE/AISI 304L austenitic stainless steels are preferred for corrosion resistance in oxidizing medias while SAE/AISI 420 martensitic stainless steels are used generally for resistance to atmospheric corrosion environments. Martensitic stainless steels exhibit high mechanical strength values close to many alloyed steels besides austenitic stainless steels present high toughness at high and low temperatures. These two different alloys may be used in a construction for economical situations and mechanical property considerations. Weld metal and heat affected zones of weldments must be thoroughly examined for discontinuities by non-destructive tests such as penetrant, ultrasonic and radiographic methods to ensure secure weldments. In this work; 304L stainless steel plates with a thickness of 3mm are joined by TIG (Tungsten Inert Gas) welding method with 3mm 420 stainless steel plates under pure argon shielding gas by 3 different TIG welding rods of ER 312, ER316L, ER2209 types. The effects of TIG welding rod compositions on weld metal defects is investigated. For this purpose, weld metals of all samples are tested by x-ray radiographic inspection method. The fewest ratios of discontinuities are detected on samples weld metals joined by ER316L TIG welding rod because of rod having the minimum amounts of chromium and the maximum amounts of nickel and consequently having the least quantities of brittle carbides as compared to samples joined by ER312 and ER2209 TIG rods.

Key Words

“Radiographic testing, 420 and 304L stainless steels, discontinuities in weld metals.”

1. Introduction

AISI/SAE 420 martensitic stainless steels have strength values close to many alloyed steels as their dominant microstructure consists of martensite while these alloys exhibit satisfactory corrosion resistance in non-aggressive medias including atmospheric corrosion. However, these steels provide less corrosion resistance values as compared to other types of stainless steels. Common applications include knives, steam, gas and jet engine turbine blades that works at low temperatures, steam pipes and valves for petroleum gatherings. The largest group of stainless steels are the austenitic alloys that cannot be transformation hardened. They can only be strengthened by cold working within the limits. The dominant microstructure is mainly austenite as referring the term austenitic. The austenitic AISI/SAE 304L alloy exhibits good low temperature high impact properties and ensures the corrosion resistance especially at oxidizing medias (ASM Vol. 2, 2005; Lippold and Kotecki, 2005).

These two different types of stainless steels have to be used together in a construction for economical, corrosion and strength considerations. These alloys are joined mainly by fusion welding processes (Lippold and Kotecki 2005; Kou, 2002).

In this study these two separate groups of alloys are joined by TIG (or also defined as; Gas Tungsten Arc Welding) welding method with three different welding rods named; ER312, ER316L and ER2209 respectively. ER312 TIG rod has mainly delta-ferritic microstructure. ER316L TIG rod has dominantly austenitic microstructure. ER2209 TIG rod has balanced delta-ferritic and austenitic microstructure. As austenitic microstructure provides more toughness on weld metals as compared to solely delta-ferritic microstructure, ER316L TIG welding rod provides more tough weld metal and less amounts of weld defects as compared to ER312 and ER2209 TIG welding rods (ASM Vol. 2, 2005; Lippold and Kotecki, 2005; Kou 2002).

Radiographic inspection is mainly preferred for more precise determination of discontinuities especially within full section of industrial parts (ASM Vol. 17, 1997; Baldev R. et.al. 2002). Numerous studies are applied on radiographic inspection of welded materials (Saravanan et.al. 2020-Tippayasam et.al. 2020). However, this study covers radiographic inspection on dissimilar TIG welding of 304L and 420 stainless steel alloys with different TIG welding rods.

In this examination; 3 mm thickness of samples from 420 and 304L alloys for 15 couples of stainless steel plates are prepared for TIG welding. Three different TIG welding rods ER312, ER316L and ER2209 are used in order to investigate the effects of the TIG rod compositions on weld defects checked by non-destructive radiographic testing method.

2. Experimental Methods

15 specimen couples in dimensions by 3x40x150mm of 420 and 304L stainless steel plates are machined for welding operations as given in Figure 1.

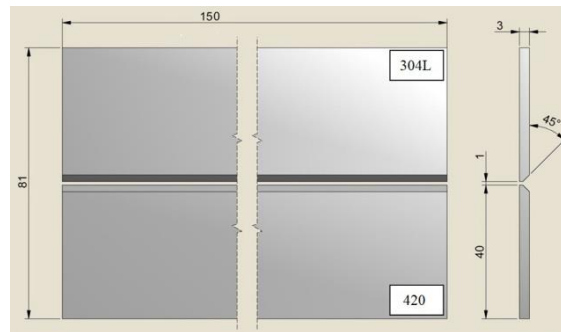


Figure 1. Samples prepared for welding operations

Optical emission spectral analysis results of 304L and 420 stainless steel raw alloys are given in Table 1. Experimental materials are consistent with the standard documents (ASM Handbook Vol. 2, 2005; ASTM A240, 2017).

Table 1. Chemical compositions of experimental materials

Material	Elements (Weight%)											
	C	Si	Mn	P	S	Cr	Mo	Ni	V	N	Fe	Others
420	0,238	0,512	0,631	0,0136	0,0023	13,37	0,0068	0,146	0,0418	0,0238	84,9	0,1147
304L	0,0241	0,374	1,18	0,0216	0,0037	18,26	0,0534	8,00	0,102	0,0684	71,6	0,3128

TIG welding is applied within two passes with direct current (-) under pure argon shielding and also backing gas. Chemical compositions of ER312, ER316L and ER2209 TIG welding rods are given in Table 2 provided from manufacturer.

Table 2. Chemical compositions of TIG welding rods provided by manufacturer

EN ISO 14343-A, AWS A5.9 TIG Rods (ISO14343,2017; AWS A.5.9, 2017)	Elements (by %weight)							
	C	Mn	Si	Ni	Cr	Mo	Cu	N
ER312	0.15<	1.6	0.4	8.8	30.7	0.2	0.14	--
ER316L	0.01<	1.7	0.4	12	18.2	2.6	0.10	0.04
ER2209	0.01<	1.5	0.5	8.5	22.7	3.2	0.01<	0.17

TIG welding operation parameters are given in Table 3.

Table 3. TIG welding parameters

TIG Welding Rod Type	Welding Current DC(-) (Amperes)		Welding Voltage (Volts)		Pure Argon Shielding Gas Flow (lt/min)		Welding Speed (mm/sec.)		TIG Welding Electrode
	Root	2 ^{nd.}	Root	2 ^{nd.}	Root	2 ^{nd.}	Root	2 ^{nd.}	
	Pass	Pass	Pass	Pass	Pass	Pass	Pass	Pass	
ER312							2.33	2.16	WT 20 (red) (2% Thoirated)
ER316L	65-70	90-95	9	11	10	6	2.29	2.18	2.4 Ø mm
ER2209							2.25	2.20	

WT20 2% thoriated welding electrode is used in joining operations. Root, final pass and backing shielding gas is pure argon. After TIG welding operation, samples are tested for discontinuities with radiographic inspection method.

The radiographic inspection instrument is MEDEX brand GEMX G-200 model and works with x-ray tube. Samples are tested by 1.2 mA current under 100kV amplitude of x-rays for 20 seconds.

3. Results and Discussion

3.1. Radiographic inspections of samples welded by ER312 TIG rod

5 samples are joined with ER312 TIG welding rod under the same welding parameters as already given in Table 3. Radiographic inspection result screens are shown in Figure 2 below.

Samples 1 and 2 among the 5 samples have exhibited no welding defects. But the remaining 3 samples have displayed (Samples 3, 4 and 5) lamellar discrete discontinuities of 70, 10 and 40 mm in lengths respectively throughout the weld centerline.

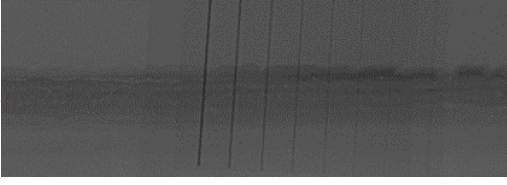
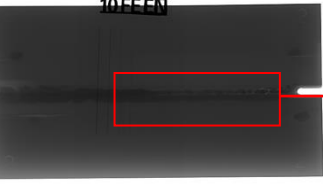
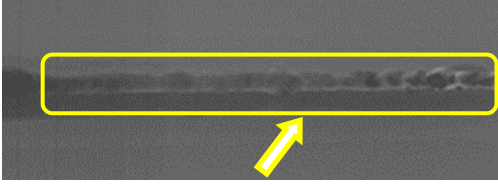
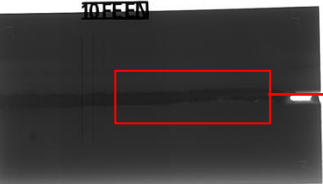
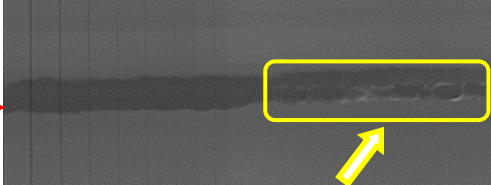
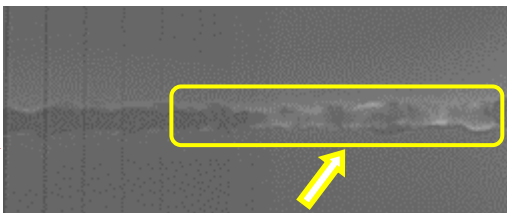
Welded Samples No.	Remarks on welded regions
 <p style="text-align: center;">Sample 1</p>	 <p style="text-align: center;">→ No discontinuity detected.</p>
 <p style="text-align: center;">Sample 2</p>	 <p style="text-align: center;">→ No discontinuity detected.</p>
 <p style="text-align: center;">Sample 3</p>	 <p style="text-align: center;">→ Lamellar discrete discontinuity length about 70 mm at the right side of weld metal detected.</p>
 <p style="text-align: center;">Sample 4</p>	 <p style="text-align: center;">→ Lamellar discrete discontinuity length about 10 mm at the right side of weld metal detected.</p>
 <p style="text-align: center;">Sample 5</p>	 <p style="text-align: center;">→ Lamellar discrete discontinuity length about 40 mm at the right side of weld metal detected.</p>

Figure 2. Radiographic inspection results of samples joined by ER312 TIG rods.

3.2. Radiographic inspections of samples welded by ER316L TIG rod

5 sample couples are joined with ER316L TIG welding rod under the same welding parameters. Radiographic inspection result screens are shown in Figure 3.

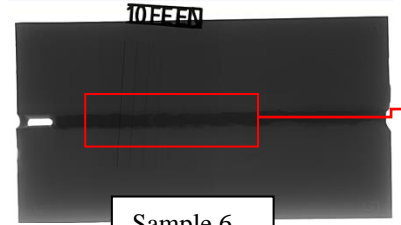
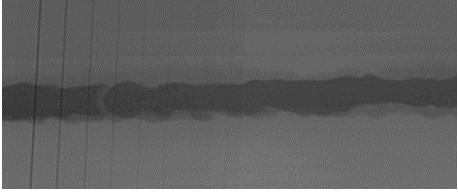
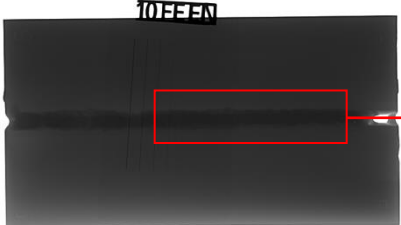
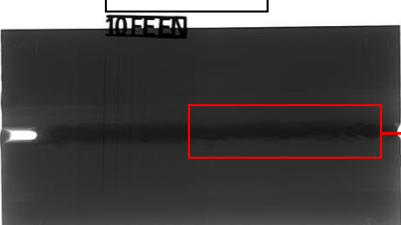
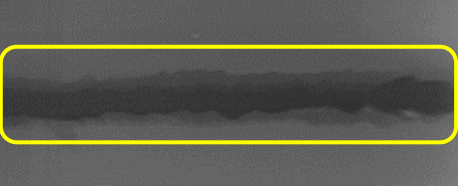
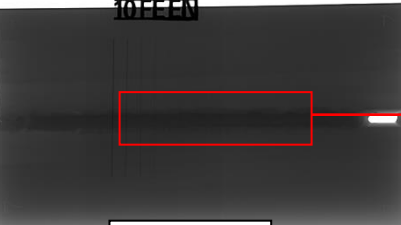
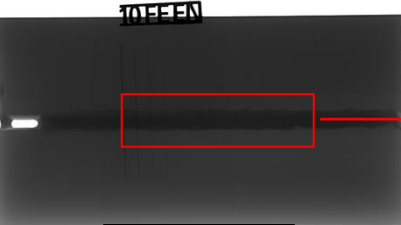
Welded Sample No.	Remarks on welded regions
 <p data-bbox="402 401 565 472">Sample 6</p>	 <p data-bbox="740 436 1040 464">→ No discontinuity detected.</p>
 <p data-bbox="402 720 565 791">Sample 7</p>	 <p data-bbox="740 716 1349 768">→ 3 spotted discrete discontinuity of 0.5mm in diameter are detected at the right hand side of weldment</p>
 <p data-bbox="402 1031 565 1102">Sample 8</p>	 <p data-bbox="740 1016 1349 1125">→ Regional seam width and thickness differences with a length about 60 mm detected at the right hand side of the weldment most probably in consequence of the changing (unstable) welding speed.</p>
 <p data-bbox="402 1367 565 1438">Sample 9</p>	 <p data-bbox="740 1394 1101 1421">→ No major discontinuity detected.</p>
 <p data-bbox="402 1682 565 1753">Sample 10</p>	 <p data-bbox="740 1709 1101 1736">→ No major discontinuity detected.</p>

Figure 3. Radiographic inspection results of samples joined by ER316L TIG rods.

3 samples (Sample No: 6, 9 and 10) have exhibited no discontinuities among the 5 samples joined by ER316L TIG Rods. However, Sample 7 has demonstrated 3 different spotted discrete discontinuities of approximately 0.5 mm in diameter while regional seam width and thickness differences with a length about 60 mm detected at the right hand side (tip end) of the Sample 8.

3.3. Radiographic inspections of samples welded by ER2209 TIG rod

Radiographic inspection result screens of 5 sample couples as welded with ER2209 TIG welding rod are shown in Figure 4.

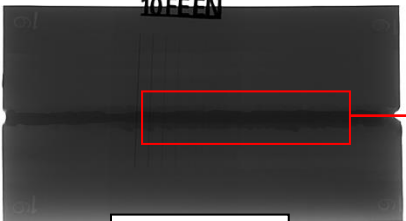
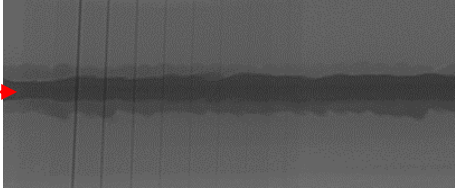
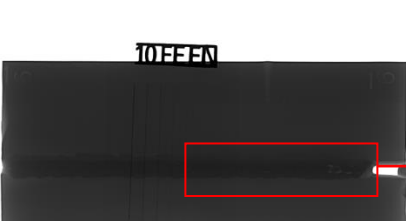
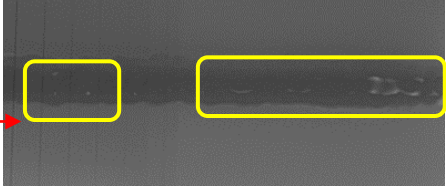
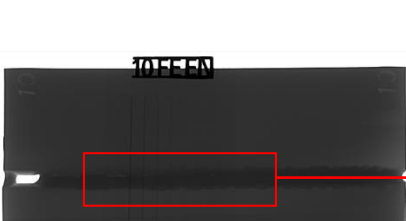
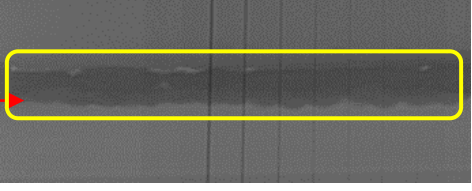
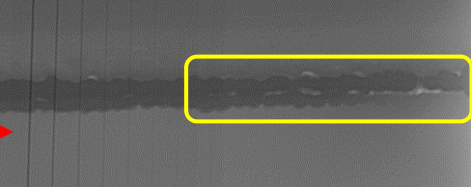
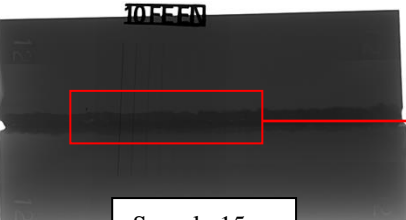
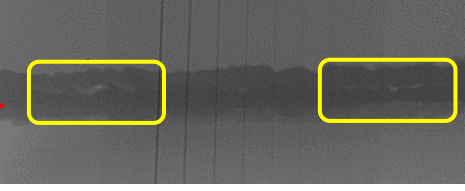
Welded Sample	Remarks on welded regions
 <p data-bbox="386 487 555 558">Sample 11</p>	 <p data-bbox="873 508 1175 537">→ No discontinuity detected.</p>
 <p data-bbox="402 814 571 886">Sample 12</p>	 <p data-bbox="704 802 1347 886">→ 4 Lamellar discrete discontinuities of length approximately about 3 mm and 2 lamellar discrete discontinuities of 1 mm in length at the left and right side of weld metal are observed.</p>
 <p data-bbox="370 1171 555 1243">Sample 13</p>	 <p data-bbox="704 1159 1347 1243">→ Lamellar discrete discontinuities with a length about 2, 8, 10 mm detected at the weld seam most probably in consequence of the changing (unstable) welding speed.</p>
 <p data-bbox="393 1528 578 1600">Sample 14</p>	 <p data-bbox="704 1507 1347 1612">→ 2 lamellar discrete discontinuities of length approximately about 2.4 mm and 2 lamellar discrete discontinuities of 4 mm in length and a long discontinuity of 28 mm at the weld metal are observed.</p>
 <p data-bbox="386 1843 555 1915">Sample 15</p>	 <p data-bbox="704 1873 1347 1927">→ 4 lamellar discrete discontinuities of length approximately about 3, 4, 8 mm at the weld metal are observed.</p>

Figure 4. Radiographic inspection results of samples joined by ER2209 TIG rods.

Sample 11 has exhibited no discontinuity among other 5 samples that joined by ER2209 TIG Rods. Sample 12 has showed 4 Lamellar discrete discontinuities of lengths approximately 3 mm and also 2 lamellar discrete discontinuities of 1 mm in length at the left and right end point side of weld metal.

Lamellar discrete discontinuities with a length about 2, 8 and 10 mm are detected at the weld seam on Sample 13. 2 lamellar discrete discontinuities of length approximately about 2.4 mm and 2 lamellar discrete discontinuities of 4 mm in length and a long discontinuity of 28 mm at the weld metal are observed on Sample 14. 4 lamellar discrete discontinuities of lengths approximately about 3, 4 and 8 mm at the weld metal are observed on Sample 15.

4. Conclusions

In this study, radiographic inspection of weld seams is made by an x-ray tube capable of producing radiographic x-rays for scanning discontinuities after joining samples by 3 different ER312, ER316L and ER2209 type TIG welding rods.

The fewest amounts of discontinuities are detected on samples weld metals joined by ER316L TIG welding rod most probably because of rod having the minimum amounts of Chromium and the maximum amounts of nickel elements as compared to ER312 and ER2209 TIG rods. Increasing amounts of chromium in weld metal forms much more chromium carbides thus these carbides are brittle in structure and may form detrimental weld defects.

On the other hand, increasing amounts of nickel element in weld metal increases toughness values. Hence ER316L TIG rod provided the minimum amounts of discontinuities on weld metals according to the radiographic test results.

On the contrary, the maximum amounts of discontinuities are detected on samples weld metals joined by ER2209 TIG rod as a result of having comparatively the highest molybdenum content and significant amounts of chromium to form brittle carbides among the other two TIG rods.

Discontinuities or weld defects in weld metals mainly forms because of improper welding parameters and unsuitable material for fusion welding. In this study, weld defects formed especially in consequence of TIG welding rod chemical composition differences.

ER316L TIG welding rod can be preferred in welding of 420 and 304L dissimilar stainless steel alloys for safely joints having the minimum amounts of weld defects according to radiographic inspection test results.

Acknowledgements

Authors express their thanks to Gazi University Welding Technologies Research and Application Center staff for radiographic testing instrument supports.

References

Abbas, M; Hamdy, AS; Essam, A. (2020). The comparison of gas tungsten arc welding and flux cored arc welding effects on dual phase steel, *Materials Research Express*, Volume 7, Issue:3, Doi: 10.1088/2053-1591/ab7f5f.

ASM Handbook Committee. (1997). *Non-Destructive Evaluation and Quality Control*, ASM Handbook Volume 17. pp. 628-761.

ASM Handbook Committee. (2005). *ASM Handbook Volume 2, Properties and Selection: Wrought Stainless Steels*, p.1303.

ASTM A240/A240M. (2017). *Standard Specification for Chromium and Chromium-Nickel Stainless Steel Plate, Sheet and Strip for Pressure Vessels and for General Applications*; ASTM International: West Conshohocken, PA, USA.

AWS A5.9/A5.9M. (2017). *Welding Consumables-Wire Electrodes, Strip Electrodes, Wires, and Rods for Arc Welding of Stainless and Heat Resisting Steels- Classification*, American Welding Society.

Baldev R. et.al. (2002). *Practical Non-Destructive Testing*, The Materials Information Society, ASM International, Narosa Publishing House, Materials Park Ohio, USA. p.54-76.

Çolak, Z; Ayan, Y; Kahraman, N. (2020). Weld morphology and mechanical performance of marine structural steel welded underwater in a real marine environment, *International Journal of Advanced Manufacturing Technology*, Volume: 109 Issue:1-2, Doi: 10.1007/s00170-020-05679-y.

Garcia-Martinez, M; Gonzalez, MPV; Meije, AG; Muro, AP. (2020). Failure Analysis of a Steel Elbow Pipe from a Gas Well, Volume 20, Issue 3, Doi: 10.1007/s11668-020-00870-5, p:723-733.

Hou, WH; Zhang, DS; Wei, Y; Guo, J; Zhang, XL. (2020). Review on Computer Aided Weld Defect Detection from Radiography Images, *Applied Sciences-Basel*, Volume 10, Issue:5, Doi: 10.3390/app10051878.

- ISO 14343. (2017). Welding consumables, Wire electrodes, strip electrodes, wires and rods for arc welding of stainless and heat resisting steels, Classification.
- J.C. Lippold, D. Kotecki. (2005). Welding Metallurgy and Weldability of Stainless Steels, Wiley Interscience, pp. 56-57.
- Kabasakaloglu, TS, Tugce S; Erdogan, M. (2020). Characterisation of figure-eight shaped oscillation laser welding behaviour of 5083 aluminium alloy, Science and Technology of Welding and Joining, 609-616, Volume:25 Issue:7, Doi: 10.1080/13621718.2020.1794652.
- Kou S. (2002). Welding Metallurgy, 2nd edition, Wiley Interscience Publications, Hoboken, NJ, USA.
- Lindner, S; Deike, R. (2020). Detection Method for Liquid Metal Embrittlement Cracks Inside the Intermediate Sheet Zone of Dissimilar Resistance Spot Welds, Steel Research International, Doi: 10.1002/srin.202000044.
- Saravanan, T; Mahadevan, S; Mukhopadhyay, CK. (2020). An improved quality assessment of fuel pin end plug welds using digital X-ray radiography, Insight, Volume: 62 Issue: 10, , 579-583, DOI: 10.1784/insi.2020.62.10.579.
- Tang, FD; Yu, Yanfeng. (2020). Nondestructive Testing Method for Welding Quality in Key Parts of Ocean-going Ships, Journal of Coastal Research, 91-94 Issue:10, Doi: 10.2112/JCR-SI110-022.1.
- Tippayasam, C.; Kaewvilai, A. (2020). Steel-Reinforced Polyethylene Pipe: Extrusion Welding, Investigation, and Mechanical Testing The effects of welding methods, with and without preheat conditions, on weld quality were investigated by visual and radiographic inspections, and crystalline analysis, Volume:99, Issue:2, Doi: 10.29391/2020.99.005.
- Yahaghi, E; Hosseini-Ashrafi ME. (2020). Comparison of the performance of three domain transform filters for radiographic contrast enhancement of welded objects, Insight, Volume: 62, Issue:6, Doi: 10.1784/insi.2020.62.6.352.